

# Directional Impedance of Geared Transmissions

by

Albert Duan Wang

S.B., Massachusetts Institute of Technology (2010)

Submitted to the Department of Mechanical Engineering  
in partial fulfillment of the requirements for the degree of

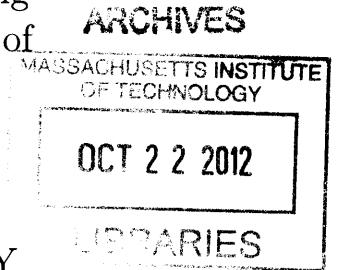
Masters of Science in Mechanical Engineering

at the

MASSACHUSETTS INSTITUTE OF TECHNOLOGY

September 2012

© Massachusetts Institute of Technology 2012. All rights reserved.



Author .....  
Department of Mechanical Engineering  
August 24, 2012

Certified by .....  
Sangbae Kim  
Esther & Harold E. Edgerton Assistant Professor of Mechanical Engineering  
Thesis Supervisor

Accepted by .....  
David E. Hardt  
Ralph E. & Eloise F. Cross Professor of Mechanical Engineering  
Chairman, Committee on Graduate Students



# Directional Impedance of Geared Transmissions

by

Albert Duan Wang

Submitted to the Department of Mechanical Engineering  
on August 24, 2012, in partial fulfillment of the  
requirements for the degree of  
Masters of Science in Mechanical Engineering

## Abstract

The purpose of this research is to develop a design tool for geared actuation systems that experience bidirectional exchange of energy with the environment. Despite the asymmetry of efficiency depending on the direction of power transfer in geared systems, typical dynamic models consider a fixed transmission efficiency for all conditions which can result in significant error depending on specific gear selection and the number of stages. This error can cause issues especially in dynamic legged robots and haptic devices when accurate force control is desired. In this paper we present directional impedance, a characteristic of geared transmissions in which the amount of power loss through the transmission differs according to the direction of power flow. Typical robots use electric motors with high gear reduction which introduces larger impedance when power flows from the output back to the motor than when the power flows from motor to output. To investigate the dependence on power flow direction, friction loss from gear teeth sliding in the gear mesh is modeled by a single gear tooth contact model and dynamic models are presented for each power transfer direction. Combinations of 0.5 mod gears were tested in experiment over a range of sizes between 16 and 120 teeth to characterize the directional effects over multiple gear selections. The experiments confirmed that for a set of differently sized gears, power loss is greater when the larger gear drives the smaller one than in the reverse case, and the asymmetry was up to 17% in the 16 and 120 tooth gear set. With a multiple stage gearbox, the difference in loss is further amplified. These findings show that directional loss in gears is a non-negligible effect and must be considered in both dynamic modeling and gear selection of robotic actuators. The gear loss model enables the modeling of motor and gearbox as a single package which can then be optimized for desired performance parameters such as peak torque, torque per mass, and mechanical impedance.

Thesis Supervisor: Sangbae Kim

Title: Esther & Harold E. Edgerton Assistant Professor of Mechanical Engineering



## **Acknowledgments**

I would like to thank my advisor Prof. Sangbae Kim for inspiration and insight during this project. I'd also like to thank Sangok Seok and National Instruments for support with LabVIEW. Prof. Jeffrey Lang and David Otten of EECS helped with motor theory and control.



# Contents

<b>1</b>	<b>Introduction</b>	<b>13</b>
<b>2</b>	<b>Theory</b>	<b>17</b>
2.1	Single Tooth Gear Contact Model . . . . .	17
2.2	Dynamics of Lossy Transmissions . . . . .	21
<b>3</b>	<b>Gear Friction Experiment</b>	<b>25</b>
3.1	Experimental Setup . . . . .	25
3.1.1	Motor Driver . . . . .	28
3.1.2	Motor Calibration . . . . .	30
3.2	Experimental Method . . . . .	31
3.3	Results . . . . .	32
3.4	A new loss model . . . . .	32
3.4.1	Direction Impedance . . . . .	34
<b>4</b>	<b>Conclusion</b>	<b>37</b>
4.1	Actuator Modeling . . . . .	37
4.2	Actuator Design . . . . .	37
4.3	Future Work . . . . .	38



# List of Figures

2-1	Force diagrams of single gear contact between two teeth. The sliding direction changes as the contact point moves past the centerline and the sliding friction force changes direction . . . . .	19
2-2	Results of the single tooth gear friction model averaged over the line of action for several combinations of input and output gear sizes. All gears are 0.5 mod and 20° pressure angle. The sliding friction coefficient is 0.3. . . . .	20
2-3	The force diagram of power flow from side 1 to side 2 through a set of gears. Loss is taken as a factor of torque entering the gear mesh that does not become amplified by the gear ratio. . . . .	23
3-1	Mechanical design of the experimental setup for testing gear friction .	26
3-2	Partially disassembled mechanical setup showing the two sets of plates, each holding a motor and driveshaft. . . . .	27
3-3	The distance between locating pins on each set of plates is used to precisely measure and set the spacing between the gears . . . . .	27

3-4	National Instruments NI cRIO-9082 chassis showing the control electronics. From left to right, the first three and last three slots house NI9505 DC Brushed Servo Drive used to drive a single phase of a three-phase brushless motor. A LEM CASR 15-NP hall effect current sensor is mounted above each motor driver and measures the current in that phase. The fourth slot is a NI 9205 analog input module used to measure the output of the current sensors. Slot 5 is a direct digital connection to the two magnetic encoders on the motor shafts. . . . .	29
3-5	The block diagram of the control algorithm used in to drive the brushless motors . . . . .	30
3-6	Loss factors of different gear pairs obtained from experiment. . . . .	32
3-7	The skew data plotted with the scaled theoretical model using friction coefficient $\mu=0.5$ and scaling the model by a factor of 100. The blue points are the skew components of the experimental data and the surface plot is the corrected model. . . . .	33
3-8	The symmetric data plotted with the theoretical model using friction coefficient $\mu=0.5$ and adding a steady state component of 0.025. The blue points are the symmetric components of the experimental data and the surface plot is the corrected model. . . . .	34

# List of Tables

- 3.1 Power loss values for several combinations of driving and driven gears. 36



# Chapter 1

## Introduction

Dynamic locomotion involves high acceleration through foot impact and alternating positive and negative work at each stride. The ability to produce correct ground reaction force depends on the actuators' mechanical characteristics. Particular to running robots and haptic displays, in which energy flows in and out of the actuator, mechanical impedance must be considered which is directly related to the passive characteristic of the actuator called 'backdrivability' [10]. The performance of force controlled manipulators and haptic devices, often evaluated by the capability of achieving prescribed impedance or force trajectories, rely heavily on the characteristics of actuators' mechanical impedance in both power transfer directions. A large component of impedance arises from the use of gearing on electric motors in typical robots.

Electromagnetic rotary motors typically used in robotics tend to produce insufficient torque for direct drive due to the thermal or magnetic field limits but they can achieve high power at high speed. As one of simplest and robust ways to obtain torque amplification and speed reduction, gearboxes are found in nearly all robotic actuators. They can transmit large torques and increase actuator torque per mass and torque per volume with greater flexibility than increasing motor size. Furthermore, major motor manufacturers offer modular gearheads of several stages with gear reductions reaching 1000:1.

In a typical high gear ratio configuration, there is little impedance from the motor

to the end effector but the gear ratio inevitably creates high impedance reflected at the end effectors. The inertia and damping on the motor shaft is reflected to the output shaft by a factor equal to the square of the gear ratio. The high impedance reduces the force transparency of the system as the motor cannot accurately sense the force put on the output shaft. For high force dynamics, there is a need for both a transparent transmission and an accurate model of how the forces are transmitted between the motor and end effector.

In addition to increasing the backdriving impedance of geared systems through reflected inertia and damping, the geared transmission itself adds impedance through friction. In highly geared systems, it is extremely difficult to backdrive the actuator. Although reflected dynamics play a role, the experiments presented in this paper show that gear friction acts asymmetrically depending on power transfer direction and increases the amount of power loss during backdriving than during times when power flows from motor to output shaft. This directional impedance phenomenon has been considered in robotic arms and compensated by adding transmission efficiency factors and switching dynamics equations depending on the state of power transfer [11]. However, it is not widely known in robotics that the asymmetry always acts to increase loss in the backdriving direction due to the geometric contact of the gears. [5] showed a torque dependent directional friction model for worm gears but did not consider spur gears used in most robots. There have also been many attempts at gear friction modeling to provide accurate models for wear and energy efficiency purposes [7] [9] [6] [1]. However, these models ignore the directional impedance effects and only consider the loss of power in a single transfer direction such from the engine of an automobile to the wheels.

Detailed gear models have not been well studied in the context of the design of highly dynamic robotics. Previous work does not provide quantitative models that specifically allow for the design and optimization of mechanical impedance of actuators. In some robots, the complexities of gear behavior have been avoided altogether using direct drive from the electromagnetic actuator [2]. Most haptic robots minimize the effect of backdrive impedance by reducing gearing or decreasing friction by em-

ploying cable transmissions. While previous work attempted to reduce transmission dynamics, the amount of force that the robot can apply is limited. The fundamental trade off is between transmission backdrive impedance and available torque. Another method introduced in the MIT Cheetah [10] is to increase the gap radius of the motor, but it is not always possible due to space constraints. This paper attempts to unify a directional gear loss model with actuator dynamics in order to provide more accurate dynamic model of behavior. When combined with an electromagnetic motor model, the motor and gear parameters can be used to determine the tradeoffs between different performance metrics. It is then possible to optimize actuator performance with a cost function that weighs the desired characteristics.



# Chapter 2

## Theory

### 2.1 Single Tooth Gear Contact Model

The involute gear tooth profile is nearly universally because the kinematic constraints enforce constant angular velocity throughout rotation. Gear teeth transmit force along the line of action where the teeth mesh. In the analysis of gear mesh friction, we make assumptions about the contact. In most spur gear sets, the contact ratio is 1.2 or greater [4]. For low contact ratios less than 1.5, a majority of the contact time is between a single tooth on each gear. Similar to the models analyzed by Anderson [1], we focused on Coulomb sliding friction between the tooth contact perpendicular to the line of action. While not containing the same complexities as existing detailed models, the simple model can be used to explain the dynamic behavior of geared systems and provide insight on the design of actuators to meet dynamic performance specifications of future robots.

The force diagram of a gear mesh is shown in Figure 2-1a. Assuming that the gears are moving at some non-zero velocity and the torques are the reaction on the gear from the shaft, the gear power loss at the output side gear soon after the driving gear tooth engages with the driven gear is shown below in Equation 2.1.

$$\lambda = \frac{\mu a(R_1 + R_2)}{R_2(\mu a + R_1 \cos(\alpha)) - \mu R_1 \sin(\alpha)} \quad (2.1)$$

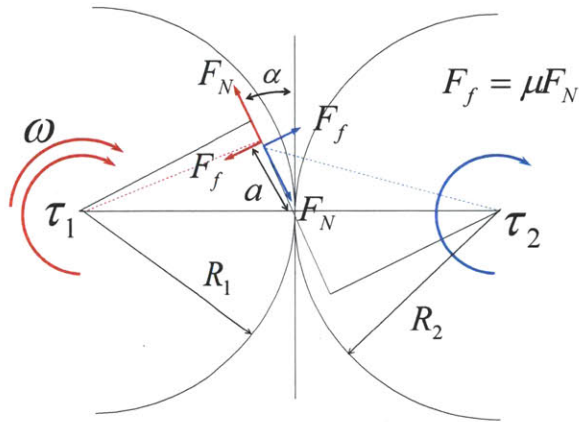
where  $\mu$  is the coefficient of sliding friction,  $a$  is the distance on the pitch line between the contact point and the center line between the two gears,  $R_1$  is the pitch radius of the driving gear,  $R_2$  is the pitch radius of the driven gear, and  $\alpha$  is the pressure angle of the gears. This equation is valid along the line of action for values of  $a$  from 0 to  $R_2 \cos(\pi/2 + \alpha) + \sqrt{R_{2,o}^2 + R_2^2 \sin^2(\alpha) - R_2^2}$  in which  $R_{2,o}$  is the outer radius of gear 2. The direction of sliding between the gear teeth changes after the contact point crosses the center line and the equation for the torque loss factor changes slightly. The force diagram is depicted in Figure 2-1a and loss factor is given equation 2.2 and is valid for  $a$  between 0 and  $R_1 \cos(\pi/2 + \alpha) + \sqrt{R_{1,o}^2 + R_1^2 \sin^2(\alpha) - R_1^2}$ .

$$\lambda = \frac{\mu a (R_1 + R_2)}{R_2 (\mu a + R_1 \cos(\alpha) + \mu R_1 \sin(\alpha))} \quad (2.2)$$

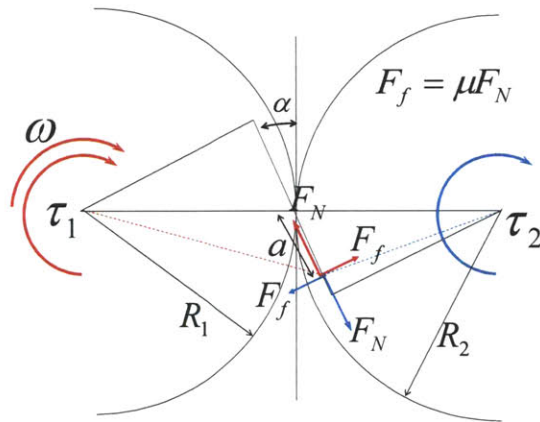
An important observation is that the gear loss is not symmetric with power direction. That is, for each set of gears the loss is different depending on which gear is the driving gear. At any given point during contact, switching the power transfer direction is equivalent to switching between equations 2.1 and 2.2 and then switching  $R_1$  and  $R_2$ . The instantaneous loss at each point along the line of action does not result in the same value for the reversed power direction.

If the model is integrated along the line of action, we obtain the contour plot of the torque loss coefficient as a function of number of teeth on the driving and driven gear shown in Figure 2-2a. The gear module is fixed at 0.5 mod and the sliding friction coefficient  $\mu$  is 0.3, a typical value for dry steel-steel contact.

The model shows that power loss in gears is highly dependent on the size of gears used. For a constant gear ratio which can be represented as a straight line from the origin on the contour plot, the amount of power loss varies with the specific size selection of the gears. In particular, using smaller gears to achieve the same gear ratio results in greater torque loss. This is due to ‘relative module’ which we define as the tooth size or module compared to the size of gear. If two gear sets have the same size gears but differing modules, the set with larger module would have a longer line of action. The length of the line of action is given by Equation 2.3 where  $R_{i,o}$  is the

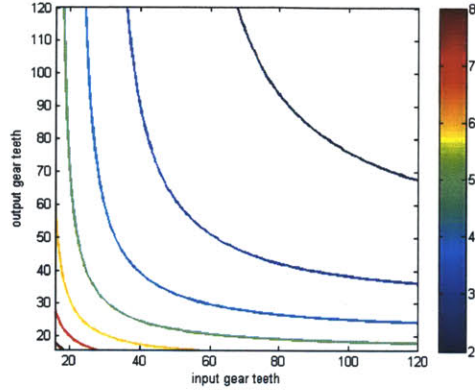


(a) Force diagram of gear teeth before the contact point reaches the centerline

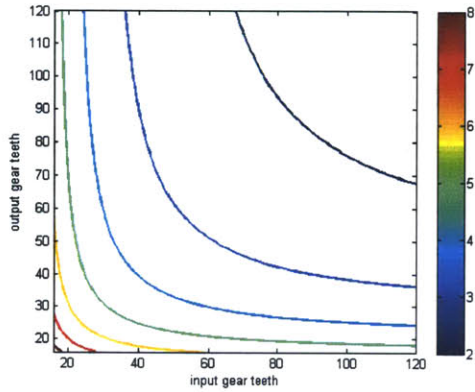


(b) Force diagram of gear teeth after the contact point passes the centerline

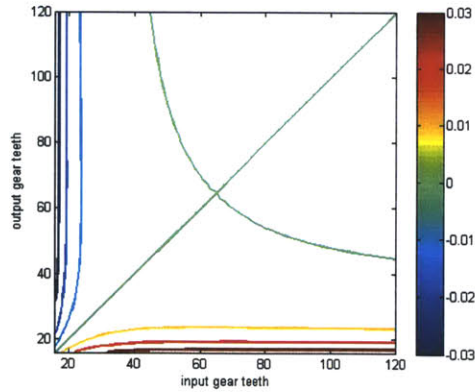
**Figure 2-1:** Force diagrams of single gear contact between two teeth. The sliding direction changes as the contact point moves past the centerline and the sliding friction force changes direction



(a) The average percentage power loss



(b) Symmetric part of average percentage loss



(c) Skew symmetric part of average percentage loss

**Figure 2-2:** Results of the single tooth gear friction model averaged over the line of action for several combinations of input and output gear sizes. All gears are 0.5 mod and  $20^\circ$  pressure angle. The sliding friction coefficient is 0.3.

outer radius and  $R_{i,base}$  is the base radius of the side  $i$  gear. In Equations 2.1 and 2.2, the greater the distance  $a$  from the centerline, the greater the torque loss. Therefore average torque loss can be reduced by using larger gears or lower module. This result is consistent with the finer teeth used on lowloss gears compared to standard gears [6].

$$\begin{aligned} \text{Length of} \\ \text{line of action} \end{aligned} = \sqrt{R_{1,o}^2 - R_{1,base}^2} + \sqrt{R_{2,o}^2 - R_{2,base}^2} - (R_1 + R_2)\sin(\alpha) \quad (2.3)$$

To better study the asymmetry in power loss in a single gear set for the two power transfer directions, the average power loss can be separated into symmetric and skew components. The values of symmetric and skew loss are calculated using Equations 2.4. The symmetric contour plot shows the average loss between the two driving cases for the same two gears. The skew component shows the deviation from the average of the two scenarios or the symmetric component. From Figure 2-2c, it is clear that for a given set of gears, there is more loss when the large gear is driving the small one. In normal gearing, the backdriving torque loss is higher, further increasing backdriving impedance compared to the forward driving. The effect is most pronounced at extreme gear ratios and there appears to be minimal difference in loss when the gears are above a certain size (30 teeth).

$$\begin{aligned} \text{Symmetric loss}(i, j) &= 0.5(\text{Loss}(i, j) + \text{Loss}(j, i)) \\ \text{Skew}(i, j) &= 0.5(\text{Loss}(i, j) - \text{Loss}(j, i)) \end{aligned} \quad (2.4)$$

## 2.2 Dynamics of Lossy Transmissions

In many cases, geared transmissions are considered without energy loss. The speed reduction and force amplification are derived from the kinematics of the gearing ratio. In this case of perfect energy transmission, the dynamics of a typical system can be

described with a familiar differential equation.

$$\tau_1 - \frac{\tau_2}{N} = (D_1 + \frac{D_2}{N^2})\omega + (J_1 + \frac{J_2}{N^2})\dot{\omega} \quad (2.5)$$

$\tau_1$  is the torque applied by the motor,  $\tau_2$  is the torque applied by the load on the output shaft,  $D_1$  is the sum of all damping on the motor shaft,  $D_2$  is the damping on the output shaft,  $J_1$  is the inertia on the motor shaft,  $J_2$  is the inertia on the output shaft,  $N$  is the gear ratio.

For applications in which backdrivability is important, the backward impedance can be minimized by keeping a low gear ratio, and by reducing the amount of damping and inertia present on the motor shaft.

In reality, transmissions must exhibit some degree of power loss from friction in the gears. Thus the expected amount of torque from the output side of the gear set should be slightly lower than what is given by kinematic velocity ratio. If it is assumed that there is some constant power loss, then there will be some asymmetry in the dynamic equations depending on the direction of power transmission. Figure 2-3 shows the dynamics when power is flowing out of the motor and to the load considering the a torque loss factor of  $\lambda$ . In the case of kinematically coupled gear transmissions, the power loss factor and torque loss factor are the same. The equations become

$$(1 - \lambda_1)\tau_1 - \frac{\tau_2}{N} = ((1 - \lambda_1)D_1 + \frac{D_2}{N^2})\omega + ((1 - \lambda_1)J_1 + \frac{J_2}{N^2})\dot{\omega} \quad (2.6)$$

for power flowing from side 1 to side 2 and

$$\tau_1 - (1 - \lambda_2)\frac{\tau_2}{N} = (D_1 + (1 - \lambda_2)\frac{D_2}{N^2})\omega + (J_1 + (1 - \lambda_2)\frac{J_2}{N^2})\dot{\omega} \quad (2.7)$$

for power flow from the side 2 to side 1.  $\lambda_1$  and  $\lambda_2$  are the torque loss factors when the power flows from side 1 and side 2 respectively. If a motor is attached to the side one shaft, the situations are analogous to acceleration and braking of a load. In order to correctly predict the behavior, the equation of motion should be switched depending on the power transfer state.

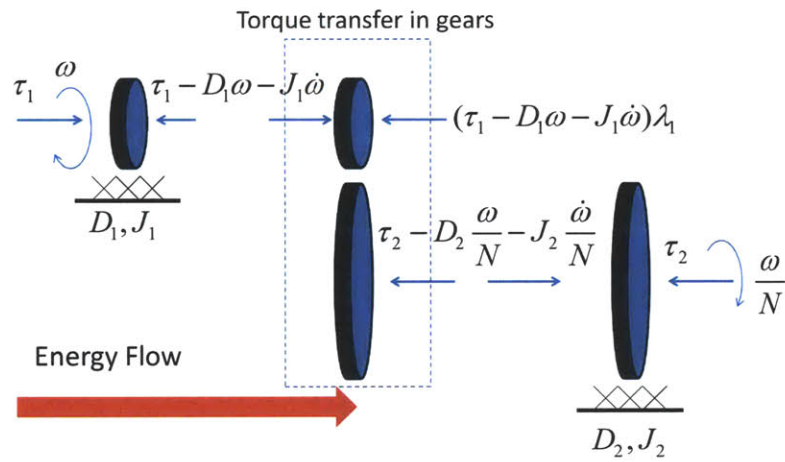


**Figure 2-3:** The force diagram of power flow from side 1 to side 2 through a set of gears. Loss is taken as a factor of torque entering the gear mesh that does not become amplified by the gear ratio.



# Chapter 3

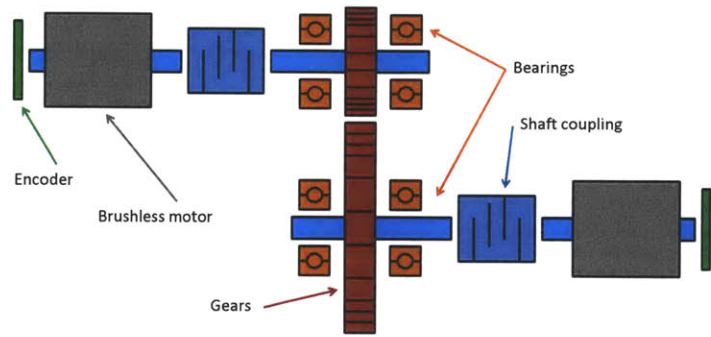
## Gear Friction Experiment

### 3.1 Experimental Setup

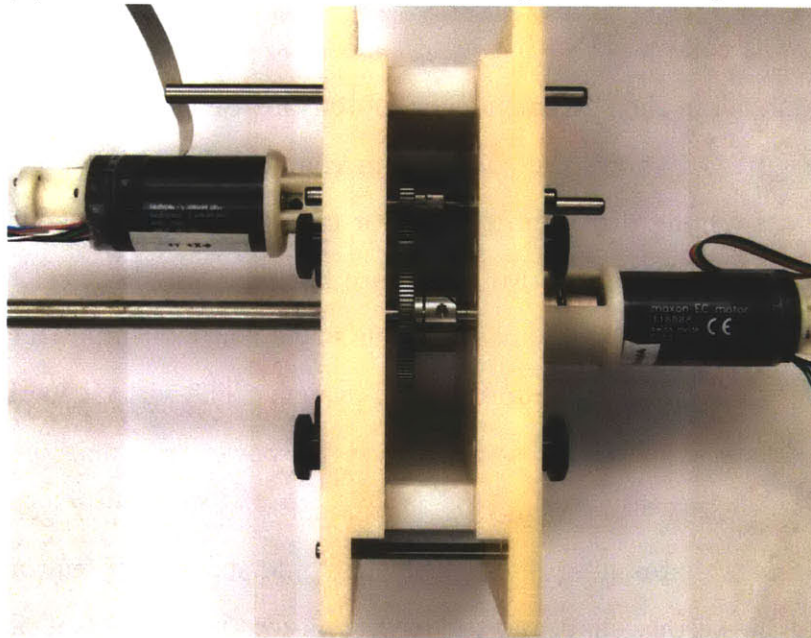
The experiment was conducted with two brushless motors driving the shafts of the two gears. By controlling the current in each motor, precise torques could be applied at each shaft. Figure 3-1 shows the complete mechanical design. Depending on the motor torque and spinning direction, one motor can act as a power source and the other as a virtual load. Since the two shafts are kinematically coupled by the gear ratio, a comparison the torques applied at each shaft can determine the amount of torque and power loss through the mechanical system. The virtual load apparatus allows the two motors to switch roles and reverse the power transmission direction.

The testing apparatus was designed to accommodate a variety of gear combinations. The two inner plates hold one motor shaft and its driving motor. The two outer plates hold the second shaft and its driving motor. In each set of plates, dowel pins are used to maintain the relative alignment of the two plates and bearings. The two sets of plates can slide relative to each other in order to precisely control the distance between the gears. Locating pins are mounted on each set of plates so that the distance between the two drive shafts can be easily measured with calipers. Figures 3-2 and 3-3 show an exploded view and the locating features respectively.

In a typical robotic actuator, the motor shaft uses a smaller gear than the output shaft to obtain torque amplification. In the forward driving case in which the motor



(a) Schematic mechanical model of the gear friction experiment



(b) Picture of the mechanical experimental setup

**Figure 3-1:** Mechanical design of the experimental setup for testing gear friction

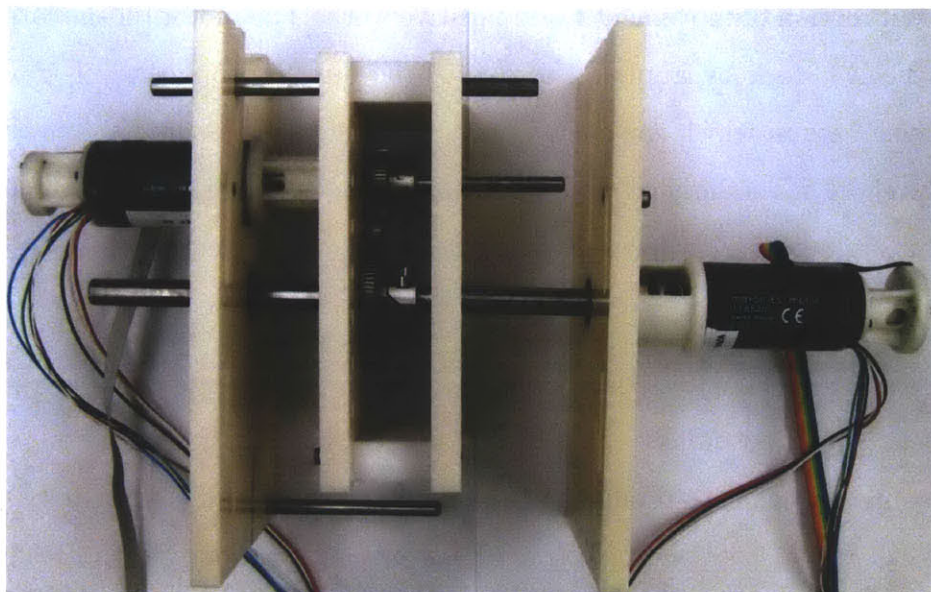


**Figure 3-2:** Partially disassembled mechanical setup showing the two sets of plates, each holding a motor and driveshaft.

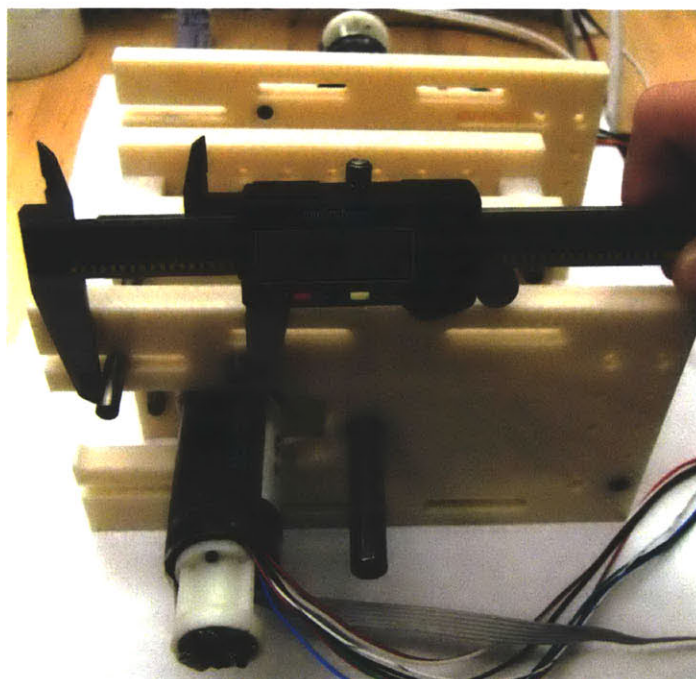


**Figure 3-3:** The distance between locating pins on each set of plates is used to precisely measure and set the spacing between the gears

power flows to some load at the output shaft, the motor on the small gear side applies torque in the direction of movement to do positive work. The motor on the large gear side does negative work by applying torque in the direction opposite of travel. In the backdriving case in which the energy flows from the load side into the motor, the motor on the shaft of the larger gear applies torque in the direction of travel and the motor on the small gear side applies torque in the opposite manner.

### 3.1.1 Motor Driver

For the experiment, sinusoidally commutated ironless brushless motors were used as the torque source in order to provide smooth torque profile. Unlike brushed DC motors, which experience torque ripple over the course of rotation due to the discrete contacts in the commutator, electrically commutated brushless motors can continuously change the direction of the magnetic field in the stator as the permanent magnets on the shaft rotate. Additionally we used an ironless motor to avoid potential cogging torque when the rotor magnets line up with the stator teeth. The particular motor chosen for the experiment was a Maxon EC32 (Order Number 118888) three-phase brushless motor. The standard method of commutating the motor uses internal hall effect sensors to measure rotor position in relation to the stator. The six different combinations of outputs dictate which wires should be connected to the positive and negative rails of the electric supply. This method, known as six-step commutation or block commutation is the easiest to implement but suffers from the torque ripple since it mimics the discrete commutation of brushed DC motors [8].

Sinusoidal commutation for brushless motors requires much more sophisticated electronics and controls compared to DC motors. All measurements must be accurate for proper force production and the challenges in calibration are described in 3.1.2. For one motor, three National Instruments NI 9505 DC Brushed Servo Drives were configured so that each driver only formed a half bridge connecting to one of the motor leads. In series with each motor lead was a LEM CASR-15NP current sensor capable of sensing bidirectional currents of 15 A. The analog outputs of the current sensor were read by an NI 9205 16-bit analog input module. Rotor position was sensed by a

RLS RMB20SC13BC10 13-bit digital magnetic encoder that sensed the position of an accompanying magnet attached to the shaft of the motor. The setup was duplicated for the second motor and all National instruments modules were mounted in a NI cRIO-9082 chassis. The control electronics are shown in Figure 3-4.

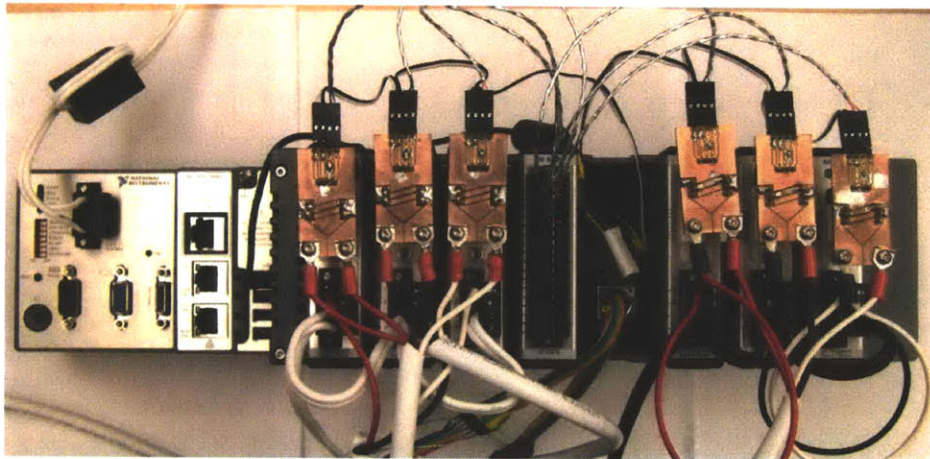


**Figure 3-4:** National Instruments NI cRIO-9082 chassis showing the control electronics. From left to right, the first three and last three slots house NI9505 DC Brushed Servo Drive used to drive a single phase of a three-phase brushless motor. A LEM CASR 15-NP hall effect current sensor is mounted above each motor driver and measures the current in that phase. The fourth slot is a NI 9205 analog input module used to measure the output of the current sensors. Slot 5 is a direct digital connection to the two magnetic encoders on the motor shafts.

The technique employed by the custom motor driver is field oriented control. During each step of the control loop, the rotor position and the three phase currents are measured and new phase voltages are issued. Using the DQ0 transformation, the Q-axis current corresponding to the torque producing current is calculated. A PI controller on Q current is then used to issue the next Q voltage command in order to regulate motor current to the set point. The Q voltage command is then transformed by the inverse DQ0 transformation to calculate new phase voltages. These voltages are then produced by the NI 9505 drivers using PWM at 20 kHz. Feedback control occurs every cycle of the PWM output. The entire algorithm was implemented on the integrated FPGA in the NI cRIO-9082 using LabVIEW. Figure 3-5 shows the architecture of the current controller.

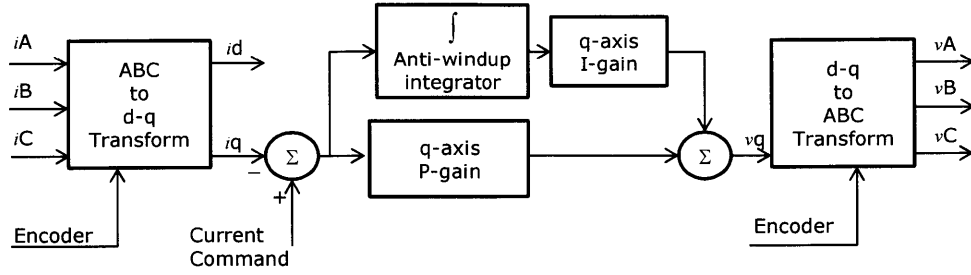


**Figure 3-5:** The block diagram of the control algorithm used in to drive the brushless motors

### 3.1.2 Motor Calibration

The two motors used for the drive source and load were calibrated to find the torque constant. The torque constant in the specification are for six step commutation and are not valid for the sinusoidal commutation used for the experiment. To find the motor constant, the motor shaft was externally driven at constant velocity and the relative voltages between the three phases were captured by oscilloscope. The motor velocity  $\omega$  was estimated from the period of the phase voltage sinusoids and the motor constant  $k$  was computed by the equations in 3.1 for back EMF of each phase. To find the torque constant using sinusoidal commutation, the torque for each phase of the motor winding is summed and given by Equation 3.2 in which  $\tau$  is the motor torque and  $I_q$  is the torque producing quadrature current calculated from the DQ0 transformation of the three phase currents.

$$\begin{cases} v_A = \omega k \cos(\theta) \\ v_B = \omega k \cos(\theta - \frac{2\pi}{3}) \\ v_C = \omega k \cos(\theta + \frac{2\pi}{3}) \end{cases} \quad (3.1)$$

$$\tau = 1.5kI_q \quad (3.2)$$

In order for the motor torque to match the calculated motor constant, the shaft position must be correctly calibrated to send the correct sinusoidal currents at each position. This procedure is conducted by removing all loads from the motor and

sending a constant current to the motor and recording the rest position of the rotor. The offset to obtain the torque calculated from the oscilloscope measurement is 90 electrical degrees so the sinusoidal pattern is advanced by 90 degrees to obtain the correct phase currents for the recorded position.

In addition to calibrating for shaft position, the current sensing in each phase of the motor must be accurate. Early experiments using low cost hall-effect current sensors suggested erroneously, that the gears were more than 100% efficient due to the sensitivity of the sensors being off by up to 7% from the stated specifications. Another issue with current sensors was drift which caused the zero current output voltage to shift over time. To ensure proper measurements, the sensitivity was verified with several test currents and each current sensor was zeroed periodically throughout the experiment.

## 3.2 Experimental Method

In the experiment, a set of gears were tested at a constant gear pitch line velocity of 500 teeth/s. The power transmitted through the gears was increased by gradually increasing the resistance torque of motor doing negative work. A PID controller on velocity was used to find the steady state torque on the driving motor to maintain the constant velocity. At constant velocity, the transmission dynamics from equations 2.6 and 2.7 simplify to

$$(1 - \lambda_1)\tau_1 - \frac{\tau_2}{N} = ((1 - \lambda_1)D_1 + \frac{D_2}{N^2})\omega \quad (3.3)$$

for energy flow from side 1 to 2 and

$$\tau_1 - (1 - \lambda_2)\frac{\tau_2}{N} = (D_1 + (1 - \lambda_2)\frac{D_2}{N^2})\omega \quad (3.4)$$

for energy flow from side 2 to 1. The torque lost through the gear mesh can be easily calculated from the slope of the output vs input torque line at constant velocity.

### 3.3 Results

Several combinations of gears were tested to find the dependence of power loss on gear size selection. All gears tested gears were 0.5 mod metric gears manufactured by Stock Drive Products/Sterling Instrument to ISO Class 7 standards. The material was 303 stainless steel and the gears were run dry. Pinion gears ranging from the 16 teeth to 40 teeth were paired with larger gears of 80, 100 and 120 teeth. During the experiment, the motor on driving gear side was used to provide positive work while the motor on the other shaft provided a load resistance. The relationship of drive torque and load torque was fit by linear least squares to obtain the slope and the loss was calculated using Equation 3.3. The loss factor of all drive combinations are shown in Table 3.1. The data are plotted in Figure 3-6.

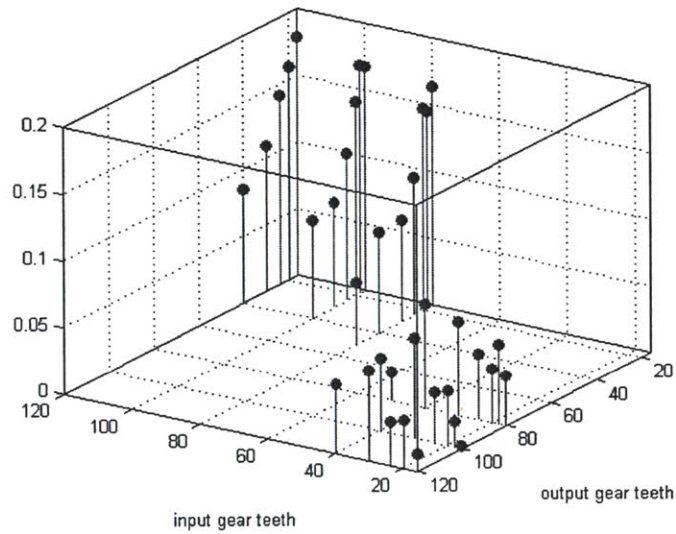


Figure 3-6: Loss factors of different gear pairs obtained from experiment.

### 3.4 A new loss model

The data has the same tendencies as the single tooth friction model in Section 2.1. However, it matches much more closely with the skew symmetric plot of loss than the total loss in Figure 2-2. In order to correct the model, we calculate the symmetric

and skew components of the data using Equation 2.4 and use them to rescale the symmetric and skew components of loss in the single tooth model.

The magnitude of the skew behavior is many times that of the theoretical model. Whereas the model predicted that the maximum component of total loss due to asymmetric loss was 0.015%, the experiment showed close to 10%. In Figure 3-7, the skew data is shown with the theoretical skew using a sliding friction coefficient of 0.5. The large friction is consistent with unhardened stainless steel to stainless steel sliding contact when the surfaces are curved in Hertzian contact as in the curved gear tooth profiles [3]. In addition, a scaling factor of 100 is applied to the theoretical model. The data matches closely with the new corrected model.

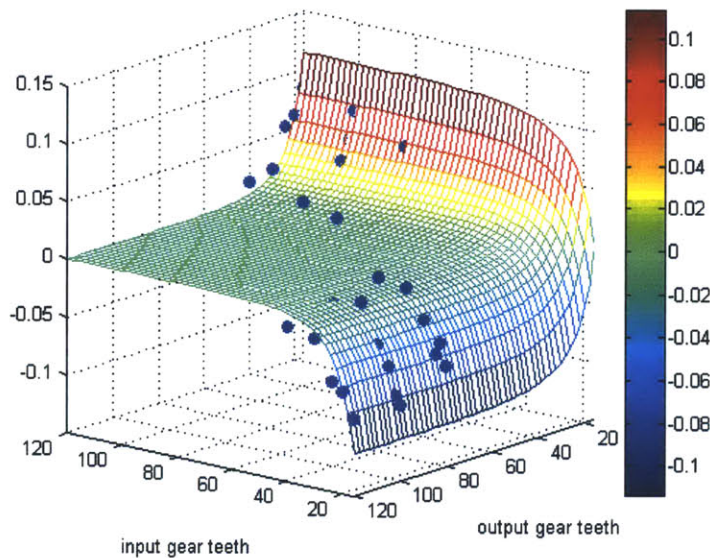


**Figure 3-7:** The skew data plotted with the scaled theoretical model using friction coefficient  $\mu=0.5$  and scaling the model by a factor of 100. The blue points are the skew components of the experimental data and the surface plot is the corrected model.

Whereas the model in Section 2.1 showed a dominant symmetric component of friction, symmetric component of the data has closer magnitude to the skew. Using the 0.5 friction coefficient that is used to fit the skew, the symmetric loss data fits the model without a scaling factor as shown in Figure 3-8. A constant term of 0.025 is added for to compensate for the steady state loss independent from gear selection. This loss is most likely caused by coulomb friction in the bearings which was not

considered in the single tooth model. The data confirms that regardless of power transfer direction, the average loss in a gear set is reduced for larger gears.

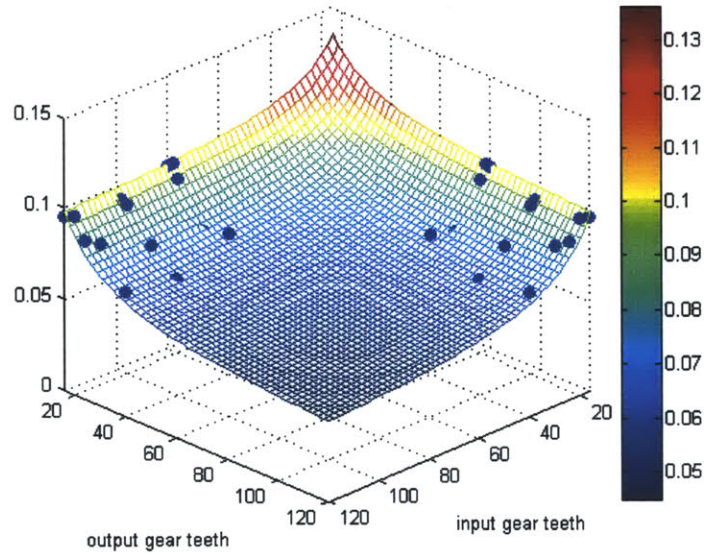


**Figure 3-8:** The symmetric data plotted with the theoretical model using friction coefficient  $\mu=0.5$  and adding a steady state component of 0.025. The blue points are the symmetric components of the experimental data and the surface plot is the corrected model.

### 3.4.1 Direction Impedance

The data clearly shows that the asymmetry of gear loss over power transfer direction in a single set of gears. In addition, the data confirms that power loss in a set of gears is always greater when the larger gear is driving the smaller one. The difference in power loss is up to 17% in the pair of gears with largest difference in size (16, 120). The asymmetry is reduced sharply as the 16 tooth gear is increased. With a 30 to 120 tooth combination, the difference in power loss is 4%. When both gears exceed 35 teeth, the magnitude of skew loss is 1%, equivalent to 2% in actual difference between the two power transfer directions. These results show that directional loss can be greatly minimized by selecting larger pinions. The tradeoff is between the impedance of larger gear inertia and directional loss.

The experimental data shows that the asymmetry is about 100 times larger than

expected from the simple single tooth model. While the trends are the same, the single tooth contact assumption is inadequate for accuracy. It is possible that the discrete contact of the second tooth may amplify the normal forces on the sliding surfaces or that other unmodeled behavior acts in the same manner as the single tooth friction model but with a larger magnitude.

**Table 3.1:** Power loss values for several combinations of driving and driven gears.

Driving gear teeth	Driven gear teeth	loss factor $\lambda$
16	80	0.037
16	100	0.001
16	120	0.013
18	80	0.059
18	100	0.019
18	120	0.024
20	80	0.040
20	100	0.041
20	120	0.036
24	80	0.049
24	100	0.038
24	120	0.032
30	80	0.070
30	100	0.075
30	120	0.068
40	80	0.078
80	16	0.163
80	18	0.150
80	20	0.147
80	24	0.102
80	30	0.078
80	40	0.075
100	16	0.167
100	18	0.144
100	20	0.170
100	24	0.109
100	30	0.077
120	16	0.179
120	18	0.159
120	24	0.142
120	30	0.109

# Chapter 4

## Conclusion

### 4.1 Actuator Modeling

The work on geared transmission dynamics presented in this thesis is useful for applications involving the control of geared systems. The results are particularly necessary for modeling dynamics of robotic systems in which the motor does both positive and negative work during acceleration and braking respectively. In these cases, the different amounts of friction loss should be incorporated into the dynamics. In experiment, the power loss values could differ by up to 17%. In applications such as automobiles in which the engine only acts mostly as a power source, the gear loss results can be applicable to accurately model the amount of torque that is transmitted to the wheels for the many gear combinations in the gearbox.

### 4.2 Actuator Design

The gear friction results presented in this paper can inform new actuator designs. The experimental data clearly showed the asymmetry of power loss depending on the power transfer direction. In running robots where backdrivability is necessary for proper energy exchange with the ground, the motor and geared transmission can be chosen to minimize the impedance while still achieving proper output torques. The results clearly show that larger gears can reduce overall friction loss, and gears more

closely matched size can reduce the amount of added friction loss in the backdriving direction when energy flows into the motor. In hybrid electric vehicles that rely on regenerative braking, the efficiency for both directions of power flow can be optimized.

### **4.3 Future Work**

The model presented in this paper makes simplifications about interaction between two gears. A more detailed model may be able account for the errors in the single tooth contact model. In the experiment, gears were run dry to easily maintain the same conditions over multiple experiments. However in application, gears are always used with lubrication and future work would examine the effects of lubricant to model more realistic operating conditions.

# Bibliography

- [1] NE Anderson and SH Loewenthal. Comparison of spur gear efficiency prediction methods. 1983.
- [2] H. Asada and K. Youcef-Toumi. *Shigley's Mechanical Engineering Design (Mcgraw-Hill Series in Mechanical Engineering)*. McGraw-Hill Science/Engineering/Math, 1986.
- [3] DH Buckley. Friction behavior of 304 stainless steel of varying hardness lubricated with benzene and some benzyl structures. (September), 1974.
- [4] Richard Budynas and Keith J. Nisbett. *Shigley's Mechanical Engineering Design (Mcgraw-Hill Series in Mechanical Engineering)*. McGraw-Hill Science/Engineering/Math, 8 edition, October 2006.
- [5] M.E. Dohring, E. Lee, and W.S. Newman. A load-dependent transmission friction model: theory and experiments. In *Robotics and Automation, 1993. Proceedings., 1993 IEEE International Conference on*, pages 430–436 vol.3, may 1993.
- [6] BR Höhn, Klaus Michaelis, and M Hinterstoisser. Optimization of gearbox efficiency. *Goriva i maziva*, pages 462–480, 2009.
- [7] Y. Michlin and V. Myunster. Determination of power losses in gear transmissions with rolling and sliding friction incorporated. *Mechanism and Machine Theory*, 37(2):167–174, February 2002.
- [8] Maxon Motor, May 2012. Sales catalog.
- [9] Chananat Ratanasumawong, Puwadon Asawapichayachot, Surin Phongsupasamit, Haruo Houjoh, and Shigeki Matsumura. Estimation of Sliding Loss in a Parallel-Axis Gear Pair. *Journal of Advanced Mechanical Design, Systems, and Manufacturing*, 6(1):88–103, 2012.
- [10] Sangok Seok, Albert Wang, David Otten, and Sangbae Kim. Actuator Design for High Force Proprioceptive Control in Fast Legged Locomotion.
- [11] E.C. Wu, J.C. Hwang, and J.T. Chladek. Fault-tolerant joint development for the Space Shuttle remote manipulator system: analysis and experiment. *IEEE Transactions on Robotics and Automation*, 9(5):675–684, 1993.